Modelling the Competitive Growth of Primary, Allotriomorphic, and Secondary Alpha in Ti-6Al-4V

RICARDO HENRIQUE BUZOLIN, DESIRÉE WEIß, ALFRED KRUMPHALS, MICHAEL LASNIK, and MARIA CECILIA POLETTI

The competitive formation of allotriomorphic α along the prior β grain boundaries, secondary α-phase and the growth of globular primary α is described for the Ti-6Al-4V alloy during continuous cooling. The formation kinetics of the different morphologies of the α-phase is related to the nucleation rate of allotriomorphic α and secondary α as well as with the V supersaturation at the β matrix. A mesoscale physical model is developed for the allotriomorphic α and secondary α based on classical nucleation and growth of platelets. The growth of the primary α is modelled as the growth of a spherical particle embedded in a supersaturated β matrix. Continuous cooling tests at two different holding temperatures in the α + β field, 930 °C and 960 °C, and five different cooling rates, 10, 30, 40, 100 and 300 °C/minutes, are conducted. Additionally, interrupted tests are conducted at different temperatures to determine the progress of growth of primary α and formation of allotriomorphic and secondary α-phases during cooling. The size of primary α increases, while its circularity decreases with decreasing cooling rate. The area fractions of primary α decrease with increasing cooling rate and increasing holding temperature. Moreover, the lower the cooling rate, the thicker the plates of allotriomorphic α and secondary α. The growth of primary α, as well as the formation of allotriomorphic α plates is observed at the beginning of the cooling stage. The formation of secondary α occurs at last and is nearly negligible for very low cooling rates. The model is able to accurately predict the different α-phase formation behaviours and the obtained results show good agreement with the experimental ones.

https://doi.org/10.1007/s11661-020-05810-4

I. INTRODUCTION

THE mechanical properties of Ti-6Al-4V, especially fatigue resistance, toughness and ductility, are strictly correlated with its microstructure formed during the industrial thermomechanical treatments.[1] Different microstructures can be achieved, *i.e.* martensitic, lamellar, equiaxed or bimodal, and they are related to the cooling rates after the thermomechanical treatment. A bimodal microstructure consisting of lamellar α and globular primary α (α_p) is usually desired because of the combination of high ductility and high toughness.[1] The globular α_p phase grows during cooling, while lamellar or secondary α (α_{SEC}) nucleates and grows at the prior β grain boundary or from the primary alpha. Moreover, a third morphology of α-phase, named allotriomorphic α (α_{GB}), also forms along the grain boundaries during cooling.

The growth of α_p phase is diffusion-controlled. For very slow cooling rates, the β-phase transforms mainly into α_p. Thus, the resulting microstructure consists of almost only large equiaxed α_p with small amounts of retained β-phase.[2] The amount of α_p decreases for increasing cooling rates and other morphologies of α-phase are formed.[3] Semiatin *et al.*[4] observed that α_p exhibits epitaxial growth for Ti-6Al-4V controlled by the diffusion of V in the β-phase. The slower the cooling the larger the range in which the growth of α_p is pronounced. The retardation and finally the end of α_p growth with decreasing temperature during cooling can be attributed to two simultaneous effects related to the formation of α_{SEC} and α_{GB}: (1) a geometric restriction for growth (pinning effect), and (2) a decrement of the supersaturation of elements in the β matrix. The matrix supersaturation is the driving force for the growth of α_p as well as for the formation of α_s and α_{GB}. In this way,

RICARDO HENRIQUE BUZOLIN, DESIRÉE WEIß, and MARIA CECILIA POLETTI are with the Christian Doppler Laboratory for Design of High-Performance Alloys by Thermomechanical Processing, Kopernikusgasse 24, 8010 Graz, Austria. and also with the Institute of Materials Science, Joining and Forming, Graz University of Technology, Kopernikusgasse 24, 8010 Graz, Austria. Contact E-mail: ricardo.buzolin@tugraz.at. ALFRED KRUMPHALS and MICHAEL LASNIK are with the voestalpine BÖHLER Aerospace GmbH & Co KG, Mariazellerstraße 25, 8605 Kapfenberg, Austria.

Manuscript submitted on December 10, 2020.
Article published online June 3, 2020

the growth of α_p competes with the formation of α_s and α_{GB} for intermediate cooling rates (between 5 and 300 °C/minutes).[5]

The presence of a rim-like region of α-phase surrounding the α_p was observed in a near-α Ti60 alloy during cooling.[3] The rim-α-phase had the same crystallographic orientation as the interior of the α_p particle, thus evidencing the epitaxial growth of the primary α-phase. Further analysis showed that the growth of α_p particles was mainly controlled by diffusion of aluminium and molybdenum for the Ti60 alloy. The nucleation rate and growth of α_{GB} depends on the cooling rate and follows a platelet-like formation.[2,4] Furthermore, extensions from α_p with same crystallographic orientation were observed preferentially along the β/β boundary suggesting formation of α_{GB} along β/β grain boundary from α_p.[3] Sun *et al.*[6] observed for a near-α alloy TA15 (Ti-6Al-2Zr-1Mo-1V) cooled from the β-phase field preferential nucleation of α_{GB} at triple junctions of the β grains, and then grew to one side of the grain boundary forming a flat plate. The α_{GB} can also nucleate from the middle of one β/β grain boundary due to high levels of local supersaturation forming an unconnected layer of α_{GB}. The formation of α_{GB} depends on the available energy and time for growth. Therefore, different morphologies of α_{GB} were observed: flat, zig-zag, and a mix of both.

Different modelling approaches were proposed for the $\beta \rightarrow \alpha$-phase transformation.[7–15] Classical Kolmogorov–Johnson–Mehl–Avrami (KJMA) equation was applied to predict the phase transformation kinetics in Ti-6Al-4V.[7] The growth of α_{GB} was modelled using the diffusion solution for the growth of plate-like particles,[8] ellipsoid particles,[8,9] and ledge growth.[8,10,11] A cellular automation model based on diffusion, mixed and interface phase transformation was proposed by Song *et al.*[12] for phase transformation in titanium alloys. Phase field models were also developed.[13–15] and showed notably accuracy to predict the growth of particles in case of complex supersaturation fields in the particle growth front.[14]

Semiatin *et al.*[4] proposed a model for the growth of α_p using the exact solutions of diffusion equations with the following considerations: (a) the diffusion coefficients were corrected with a thermodynamic factor for the specific composition of the material, and (b) the supersaturation degree reached during cooling is the driving force for the diffusion process.[4] Meng *et al.*[16] complemented the model proposed by Semiatin *et al.*[4] by considering the effect of thermal history on the diffusion field around the α_p and the overlap of diffusion fields of growing phases.[17]

Extensive modelling of the formation of α_{SEC} was performed by Katzarov *et al.*[18] The morphology, distribution, and geometry of the α_{SEC} was simulated using finite element modelling implemented to solve the diffusion equation on the domain occupied by the β-phase. A random nucleation model as a function of the supersaturation of V in the matrix was implemented for 1-D and 2-D simulations of the formation of α_{SEC}. It was observed that lower cooling rates lead to faster transformation of $\beta \rightarrow \alpha_{SEC}$, considering the same temperature. Additionally, the thickness dependency of the α_{SEC} on temperature during isothermal treatment was also measured and simulated. Despite the broad capability of prediction of the model proposed by Katzarov *et al.*,[18] the model was developed only for $\beta \rightarrow \alpha$ transformation from the β field and not from the $\alpha + \beta$ field. Using a similar approach, the precipitation of α_{SEC} in competition with the epitaxial growth of α_p was modelled and simulated for a TA15 alloy.[5] In this case, the diffusion of Mo in β-phase was the controlling mechanisms for $\beta \rightarrow \alpha$ transformation. The growth of α_{SEC} was proposed to be a competition between direct interference from interface stability, where no misorientation is observed between the nucleating plate and the substrate, and sympathetic nucleation, where low-angle boundaries exist between the nucleating plate and the pre-existing substrate.

Robust, accurate and computational simple models to simulate the $\beta \rightarrow \alpha$ transformation are necessary to predict and control the evolution of the microstructure in components with complex shapes produced by thermomechanical processing. Here we propose a simple model that is able to couple the competitive growth of primary α and formation of allotriomorphic α as well as secondary α-phases. The results are compared with systematic measured data acquired for different continuous cooling experiments below the β-transus temperature.

II. EXPERIMENTAL PROCEDURES

A. *Material*

A cogged Ti-6Al-4V in the β and $\alpha + \beta$ fields with further annealing at 730 °C for 1 hour followed by air cooling was used for this investigation. The β-transus calculated using JMatPro® v.10 is ~995 °C and the chemical composition is listed in Table I.[19] Cylindrical samples with a diameter of 5.5 mm and a length 10 mm were heat treated in a dilatometer.

B. *Heat Treatments*

A dilatometer DIL 805A/D (TA Instruments, Hüllhorst, Germany) was used to perform continuous cooling heat treatments. The tests were carried out in a protective atmosphere of argon. After heating with a rate of 30 °C/minutes, the samples were held for 1 hour at two different holding temperatures in the $\alpha + \beta$ field, 930 °C and 960 °C, and then continuously cooled up to room temperature. The cooling was conducted using five different cooling rates: 10, 30, 40, 100 and 300 °C/minutes. Interrupted continuous cooling heat treatments were carried out to elucidate the mechanism/s governing the $\beta \rightarrow \alpha$ transformation during cooling. After heating with 30 °C/minutes, the samples were held for 1 hour at a constant temperature of 960 °C. The subsequent cooling was performed with 10 and 100 °C/minutes. The samples were quenched using argon flow for four different temperatures, 900, 875, 850 and 800 °C.

C. *Metallography and Microstructure Investigation*

The samples were polished using OP-S (oxide polishing suspension) after a conventional grinding procedure from grit 500 up to 2000. The samples were etched with the Kroll's reagent: 91 ml water, 6 ml HNO_3 (69 vol Pct) and 3 ml HF (40 vol Pct). The prepared samples were investigated using light optical (LOM) and scanning electron (SEM) microscopy. A minimum of five representative LOM micrographs were analysed for each cooling rate and holding temperature for quantification of the globular α_p. The thickness of α_{GB} as well as of α_{SEC} were measured following the stereology procedures for quantification described by Tiley *et al.*[20] For comparison, the interspace distance between the lamellas of α_{SEC} and the thickness of α_{GB} were manually measured to obtain a thickness distribution. For each micrograph, the particles of α_p were manually marked using software GIMP (GNU Image Manipulation Program)[21] and analysed using ImageJ software.[22] The SEM analyses were conducted using a Tescan Mira3 microscope equipped with a Hikari EBSD camera. SE images were acquired using an acceleration voltage of 10 kV and a working distance of 12 mm. A minimum of five representative SE micrographs were acquired to measure the thickness of α_{GB} and α_{SEC}. An acceleration voltage of 25 kV and a working distance of 15 mm were used for the EBSD measurements. An area of 200 μm x 200 μm was measured using a step size of 0.2 μm. The data treatment was performed using the OIM DataAnalysis® software. A confidence index standardization was performed considering a minimum grain size of ten points and minimum boundary misorientation angle of 12 deg. Finally, the neighbour confidence index correlation was used to re-index the data-points with confidence index lower than 0.75.

Table I. Chemical Composition of the Investigated Ti-6Al-4V [Weight Percent][19]

Al	V	Fe	O	C	N	H	Y
6.54	4.21	0.20	0.185	0.028	0.023	0.000335	< 0.001

D. *Modelling Strategy*

In the proposed model, the formation of α_{SEC}, α_{GB} and α_p is computed simultaneously. The implementation is detailed and are separated mainly on nucleation kinetics (does not apply for the α_p) and growth kinetics. The growth of α_p during cooling in heat treatments conducted below the β-transus temperature was modelled based on Reference 4. The growth of α_{GB} and α_{SEC} were modelled based on the classical model of nucleation and diffusion equation for the growth of a platelet.[5] The microstructure is modelled as consisted of three major morphologies of α-phase: α_p, α_{SEC} and α_{GB}, all embedded in a β-phase matrix, as schematically shown in Figure 1.

1. *Growth of primary alpha (α_P)*

Semiatin *et al.*[4] showed that for Ti-6Al-4V the growth of globular α_p phase during cooling is limited only by V diffusion due to supersaturation. The interdiffusion coefficient of V in β titanium D_V^{β} as a function of temperature T is calculated from Reference 23 and also adopted in the model of Semiatin *et al.*[4] as well as Villa *et al.*[24] Eq. [1].

$$D(\mu m^2/s) = 1 \times 10^5 exp - \frac{17460}{T} \qquad [1]$$

The growth of a spherical particle embedded in an infinite matrix of composition C_M is given according to Eq. [2].

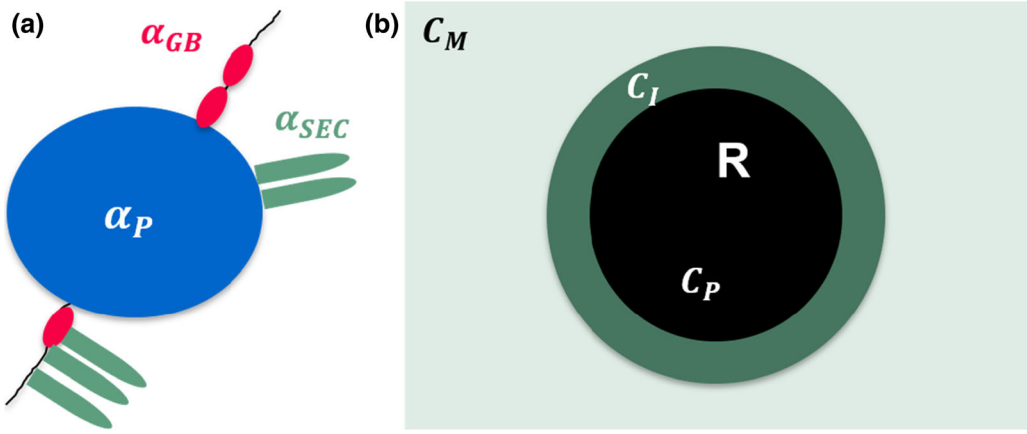

Fig. 1—(*a*) Schematic representation of the different morphologies of α-phase: primary (α_p), secondary (α_{SEC}) and allotriomorphic (α_{GB}), formed during cooling for a typical Ti-6Al-4V alloy; (*b*) growth of a spherical particle of radius R and particle composition C_P embedded in an infinite matrix of composition C_M, in which C_I is the chemical composition of the matrix at the interface.

$$\frac{dR}{dt} = 2\lambda^2 \frac{D}{R} \quad [2]$$

where R is the radius of the particle, D is the diffusion coefficient and is a growth rate parameter denoting the interface α_P/β and is calculated according to Eq. [3].

$$\left\{\lambda^2 e^{\lambda^2}\right\}\left[e^{-\lambda^2} - \lambda\pi^{1/2} erfc(\lambda)\right] = \frac{\Omega}{2} \quad [3]$$

The parameter Ω denotes supersaturation and is calculated according to Eq. [4].

$$\Omega = \frac{(C_M - C_I)}{(C_p - C_I)} \quad [4]$$

where C_I is the composition of the matrix-α_P interface and C_P is the composition of the α_p phase. C_I is considered as the equilibrium phase composition obtained from the phase diagram of the alloy at the calculated temperature considering a diffusion-controlled reaction,[4] and C_P is considered as the equilibrium phase composition of the α-phase obtained from the phase diagram. It is considered a constant value with respect to temperature[4] and equivalent to the V concentration in α-phase.[4] Following this assumption, all α morphologies have same C_P. The compositions are given in wt.Pct.

The supersaturation is the driving force for the growth of α_p. The α-phase fraction at equilibrium as well as the chemical composition (C_I) was calculated using the software JMatPro® v.10 in wt.Pct and are shown in Figures 2(a) and (b), respectively. To account for the soft impingement on the "far-field" matrix composition, C_M is calculated using a usual mass balance between the total fraction of α (f_α) phase, as given in Eq. [5].

$$C_M = \frac{(C_0 - f_\alpha - C_\alpha)}{(1 - f_\alpha)} \quad [5]$$

C_0 is the nominal concentration of V in the material.

2. *Formation of allotriomorphic alpha (α_{GB})*

Similar to the growth of α_p, the partial enrichment of V along the formed α/β-phase boundary is observed. Due to high anisotropy in interfacial energy a plate-like morphology of the α-phase is observed to form along the β/β grain boundaries. In the present model, the lengthening is considered notably higher in comparison to the thickening as also suggested by phase field simulation.[25] Therefore, the increase in the volume fraction of α_{SEC} or α_{GB} originates mainly from increase in number density and their thickness.[5] The nucleation, growth and overall transformation kinetics of grain boundary allotriomorphic platelets were proposed for steels[26] and titanium alloys.[27] Following a similar approach, when the nucleation time is neglected, the nucleation rate of precipitates is given according to Eq. [6].

$$\frac{dN_{GB}}{d_t} = N_{0GB}(1 - f_{\alpha p} - f_{\alpha GB} - f_{\alpha SEC}) \exp\left(\frac{Q}{RT}\right) \exp\left(-\frac{\Delta G^*_{NucGB}}{RT}\right) \quad [6]$$

where N_{0GB} is a pre-exponent term corresponding to the number of incubation sites multiplied by a constant[18] and fitted according to an empirical power law to account to the effect of the initial prior beta grain size, Eq. [7]. Q is the activation energy for atomic migration across the interface and assumed to be half of the activation energy for diffusion.[28,29] ΔG^*_{NucGB} is the energy barrier for heterogeneous nucleation, R the molar gas constant and T the temperature. $f_{\alpha p}$, $f_{\alpha GB}$ and $f_{\alpha SEC}$ are the calculated volume fraction of α_p, α_{GB} and α_{SEC}, respectively, and their sum is the total fraction of alpha phase (f_α).

$$N_{0GB} = 6.9 \times 10^4 \left(\frac{GS_0}{GS}\right)^{0.5} \quad [7]$$

where GS_0 is a reference grain size and considered as 35 μm in the current model and GS is the prior beta grain size. The energy barrier for heterogeneous nucleation of α_{GB} is calculated according to Eq. [8].

$$\Delta G^*_{NucGB} = -\frac{(A^*_{GB})^3}{(RT)^2\left[\ln\left(\frac{C_M}{C_I}\right)\right]^2} \quad [8]$$

where A^*_{GB} is a parameter obtained according to the nucleation at grain boundary ($A_{\alpha\beta}$), or sympathetic nucleation (A_{SYM}),[5] or a sum of contributions of both (adopted in the current model), Eq. [9].

$$A^*_{GB} = 0.12A_{SYM} + 0.88A_{\alpha\beta} \quad [9]$$

where

$$A_{SYM} = \left(4\pi N_A \gamma^2_{\alpha\beta}\gamma_{\alpha\alpha} V^2_m\right)^{1/3} \quad [10]$$

$$A_{\alpha\beta} = \left(\frac{16\pi N_A \gamma^3_{\alpha\beta} S(\theta) V^2_m}{3}\right)^{1/3} \quad [11]$$

where N_A is the Avogadro constant ($N_A = 6.02214076 \times 10^{23} mol^{-1}$), $\gamma_{\alpha\beta}$ is the interface energy between α/β-phases and considered $\gamma_{\alpha\beta}$ =0.10 J/m^2.[18] $\gamma_{\alpha\alpha}$ is the interface energy of α/α-phase and

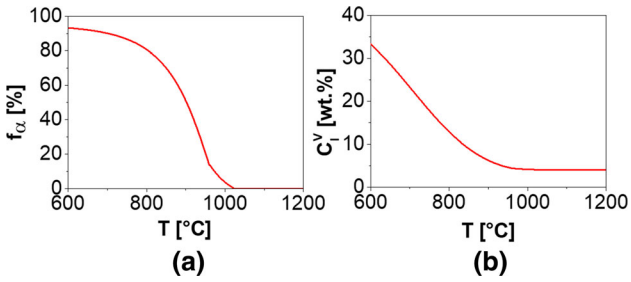

Fig. 2—Simulated data using JMatPro® v.10: (*a*) equilibrium α-phase fraction; (*b*) equilibrium V concentration for the β matrix obtained from the phase diagram.

$\gamma_{\alpha\alpha}$ =0.30 J/m^2.[5] V_m is the atomic volume of Ti ($V_m = 1.0896 \times 10^{-5}$ m^{3}mol^{-1}) and $S(\theta)$ is a shape factor given as a function of the wetting angle of the optimum embryo shape.[18] $\gamma_{\alpha\beta}(S(\theta))^{1/3} = 0.012$ Jm^{-2}.[18] A small variation in the interface energies ($\gamma_{\alpha\beta}$ or $\gamma_{\alpha\alpha}$) notable impacts the nucleation rate. In the case of the sympathetic nucleation, A_{SYM} is a function of both, $\gamma_{\alpha\beta}$ (second order) and $\gamma_{\alpha\alpha}$ (first order). On the other hand, for nucleation at grain boundary, $A_{\alpha\beta}$ is a function of only $\gamma_{\alpha\beta}$ (third order). Thus, a small increase or decrease in $\gamma_{\alpha\beta}$ and $\gamma_{\alpha\alpha}$ would affect notably A_{SYM} and/or $A_{\alpha\beta}$, increasing or decreasing the nucleation rate significantly, respectively. Finally, the model is adjusted with respect to the measured data as shown in Eq. [9] where a weighted sum of both A_{SYM} and $A_{\alpha\beta}$ is considered. The critical thickness (B_{GBcrit}) for a disc-like α_{GB} to nucleate is calculated according to Eq. [12].

$$B_{GBcrit} = -\frac{4\gamma_{\alpha\beta}}{\Delta G_{VGB}} \quad [12]$$

where ΔG_{VGB} is the chemical free energy of phase transformation obtained using Eq. [13].[5]

$$\Delta G_{VGB} = \frac{C_I - C_P^{\alpha_{GB}}}{1 - C_I} \frac{RT}{\left(1 + \frac{\partial V}{\partial C_I}\frac{C_I}{V}\right)} \ln\left(\frac{C_I}{C_M}\right) \quad [13]$$

$C_P^{\alpha_{GB}}$ is the concentration of V in the α_{GB} assumed equal to the V concentration in the α_p ($C_P^{\alpha_{GB}} = C_P$).

If the misfit strain energy is ignored, the nucleus of α_{GB} grows by diffusion process by thickening of a planar disordered boundary *via* ledge growth mechanism. The lengthening of a platelet is significantly faster than the thickening due to high anisotropy in interfacial energy. Therefore, the evolution in the volume fraction of α_{GB} is only dependent on the variation of the number density of α_{GB} and its thickness. The variation in number density is related to the number of nuclei and calculated according to Eq. [6]. The thickening of the α_{GB} is modelled according to Eq. [14].

$$\frac{dB_{GB}}{dt} = \frac{2m_{GB}\lambda_{GB}^2 D}{B_{GB}} \quad [14]$$

where B_{GB} is the thickness of the α_{GB}, m_{GB} is a ledge coefficient to account for the planar disordered growth[5] and fitted as 5 for the investigated alloy, D is the diffusivity of V in the β matrix and λ_{GB} is a growth rate parameter denoting the interface α_{SEC}/β and is calculated according to Eq. [15].

$$\pi^{1/2}\exp(\lambda_{GB}^2)erfc(\lambda_{GB}) = \Omega_{\alpha GB} \quad [15]$$

where $\Omega_{\alpha GB} = (C_I - C_M)/\left(C_I - C_P^{\alpha_{GB}}\right)$ is a dimensionless supersaturation parameter, and considered equal to Ω because $C_P^{\alpha_{GB}} = C_P^{\alpha_p}$. Similar to the growth of precipitates, the mean thickness of the platelets is calculated according to Eq. [16].[25]

$$\frac{d\bar{B}_{GB}}{dt} = \frac{dB_{GB}}{dt} + \frac{1}{N_{GB}}\frac{dN_{GB}}{dt}(B_{GBcrit} - \bar{B}_{GB}) \quad [16]$$

The first term corresponds to the growth of the existing platelets of α_{GB}, while the second one represents the contribution of new nuclei of critical size calculated according to Eq. [12]. The overall fraction of α_{GB} is calculating according to Eq. [17].

$$f_{\alpha GB} = N_{GB}\bar{B}_{GB} \quad [17]$$

The parameters used for the simulation of the formation of α_{GB} are listed Table A1.

3. *Formation of secondary alpha (α_{SEC})*

The formation of α_{SEC} is modelled similar to the formation of α_{GB}, *i.e.* nucleation of disc platelets and growth. The colony size is not modelled, but only the thickness of the formed α_{SEC} platelets and its number density (interpreted as the total number of formed nuclei of α_{SEC}). The lengthening is considered notably faster in comparison to the thickening of the α_{SEC}, thus neglected. Due to high anisotropy in interfacial energy, platelet-like α_{SEC} is formed. Differently from the growth of α_{GB} that is along the β/β grain boundaries, the growth of α_{SEC} occurs from the grain boundary towards the centre of the prior β grain as well as sympathetic growth from the α_p. Not considering any nucleation time, the rate of nucleation of α_{SEC} is given according to Eq. [18].

$$\frac{dN_{SEC}}{dt} = N_{0SEC}\left(1 - f_{\alpha p} - f_{\alpha GB} - f_{\alpha SEC}\right) \exp\left(-\frac{Q}{RT}\right)\exp\left(-\frac{\Delta G_{NucSEC}^*}{RT}\right) \quad [18]$$

where N_{0SEC} is a pre-exponent term similar to N_{0GB} and fitted as $6 \times 10^7 \times \Delta G_{NucSEC}^*$ is the energy barrier for heterogeneous nucleation of the α_{SEC} and calculated according to Eq. [19].

$$\Delta G_{NucSEC}^* = -\frac{\left(A_{SEC}^*\right)^3}{(RT)^2\left[\ln\left(\frac{C_M}{C_I}\right)\right]^2} \quad [19]$$

where A_{SEC}^* is fitted and calculated according to Eq. [20].

$$A_{SEC}^* = 0.56A_{SYM} + 0.44A_{\alpha\beta} \quad [20]$$

The critical thickness ($B_{critSEC}$) for a disc-like α_{SEC} to nucleate is calculated according to Eq. [21].

$$B_{SECcrit} = -\frac{4\gamma_{\alpha\beta}}{\Delta G_{VSEC}} \quad [21]$$

where $\gamma_{\alpha\beta}$ is the interface energy between α and β-phases, ΔG_{VSEC} is the chemical free energy of phase transformation of α_{SEC} obtained using Eq. [22].[5]

$$\Delta G_{VSEC} = \frac{C_I - C_P^{\alpha_{SEC}}}{1 - C_I} \frac{RT}{\left(1 + \frac{\partial V}{\partial C_I}\frac{C_I}{V}\right)} \ln\left(\frac{C_I}{C_M}\right) \quad [22]$$

$C_P^{\alpha_{SEC}}$ is the concentration of V in the α_{SEC}, considered to be equal to the V concentration in the α_p and α_{GB} ($C_P^{\alpha_{SEC}} = C_P^{\alpha_{GB}} = C_P$).

The growth of the nucleus of α_{SEC} is modelled as the growth of the α_{GB}. The thickening of the α_{SEC} is given according to Eq. [23].

$$\frac{dB_{SEC}}{dt} = \frac{2m_{SEC}\lambda_{SEC}^2 D}{B_{SEC}} \quad [23]$$

where B_{SEC} is the thickness of the α_{SEC}, m_{SEC} is a ledge coefficient and fitted as 3 for the investigated alloy, D is the diffusivity of V in the β matrix and λ_{SEC} is a parameter denoting the interface α_{SEC}/β that is calculated according to Eq. [24].

$$\pi^{1/2}\exp(\lambda_{SEC}^2)erfc(\lambda_{SEC}) = \Omega_{\alpha SEC} \quad [24]$$

where $\Omega_{\alpha SEC} = (C_I - C_M)/(C_I - C_P^{\alpha_{SEC}})$ is a dimensionless supersaturation parameter. The mean thickness of the α_{SEC} is calculated according to Eq. [25].[30]

$$\frac{d\bar{B}_{SEC}}{dt} = \frac{dB_{SEC}}{dt} + \frac{1}{N_{SEC}}\frac{dN_{SEC}}{dt}(B_{SECcrit} - \bar{B}_{SEC}) \quad [25]$$

The first term corresponds to the growth of the existing platelets of α_{SEC}, while the second represents the contribution of new nuclei of critical size calculated according to Eq. [21]. The overall fraction of α_{SEC} is calculating according to Eq. [26].

$$f_{\alpha SEC} = N_{SEC}\bar{B}_{SEC} \quad [26]$$

The parameters used for the simulation of the formation of α_{SEC} are listed Table A1.

III. RESULTS AND DISCUSSION

Figures 3(a) and (b) show representative microstructures of the Ti-6Al-4V argon quenched after holding at 930 °C and 960 °C for 1 hour, respectively. The measured area fractions of α_p are 38.6 ± 2.8 and 18.2 ± 3.3 Pct for the heat treatment at 930 °C and 960 °C, respectively. Sparsely and nearly separated α_p particles are found in a matrix of martensite (α'), originally a matrix of β-phase. The partial agglomeration of α_p is higher for the heat treatment at 930 °C, Figure 3(a). No trace of α_{SEC} is observed. However, the α_p particles slightly deviates from an ideal spherical shape particle.

A. *Experimental Observations*

1. *Influence of the Cooling Rate*

Representative micrographs of the continuously cooled microstructure after holding for 1 hour at 930 °C and 960 °C are shown in Figure 4. The cooling rate of 10 °C/minutes leads to a nearly fully equiaxed microstructure in both cases. The shape of the α_p exhibits higher irregularities in the case of 960 °C, decreasing its circularity. It is difficult to distinguish the lamellas of α_{SEC} or α_{GB} from the globular α_p for samples cooled down at 10 °C/minutes. The growth of α_p is also observed for the cooling rate of 30 °C/minutes. The increase in cooling rate leads to a clear formation of α_{SEC}, as well as of α_{GB} phase. For 30 °C/minutes, α_{GB} exhibits bulges, as well as the α_p phase. Higher cooling rates lead to less pronounced growth of α_p.

A detailed analysis of the microstructure after continuous cooling from 930 °C and 960 °C is seen in the SE micrographs of Figure 5. The α_{GB} and α_{SEC} are highlighted in dashed red and green lines, respectively. For the cooling rate of 300 °C/minutes, the presence of very fine acicular-like martensite (α') is marked in yellow and in its vicinity plate-like α_{SEC} is also observed. The morphology of α_{SEC} deviates slightly from an ideal flat plate-like morphology. Serrations and discontinuous interlamellar β-phase are observed, especially for the cooling rate of 30 °C/minutes. Moreover, the above-mentioned irregularities of the shape of α_P and α_{GB} are observed. The serrations at the interfaces of α_P are related to the surface instability due to competitive growth of α_{GB}, α_{SEC} and α_P. When the α_{SEC} or α_{GB} are formed in the vicinity of an α_P particle, it either hinders the local movement of the interface of the α_P and/or changes the supersaturation for its growth. Comparably, if α_{SEC} nucleates from α_{GB} it also changes its interface movement kinetics and supersaturation field

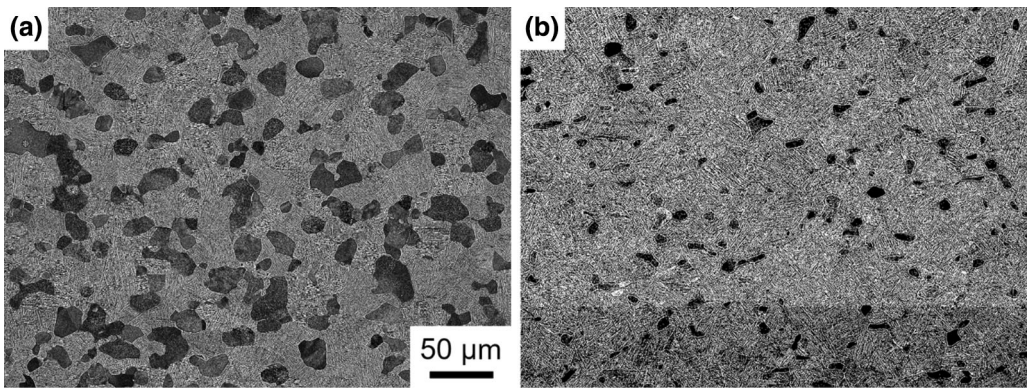

Fig. 3—Representative BSE micrographs of the investigated Ti-6Al-4V after 1 h at (*a*) 930 °C followed by argon quenching; (*b*) 960 °C followed by argon quenching.

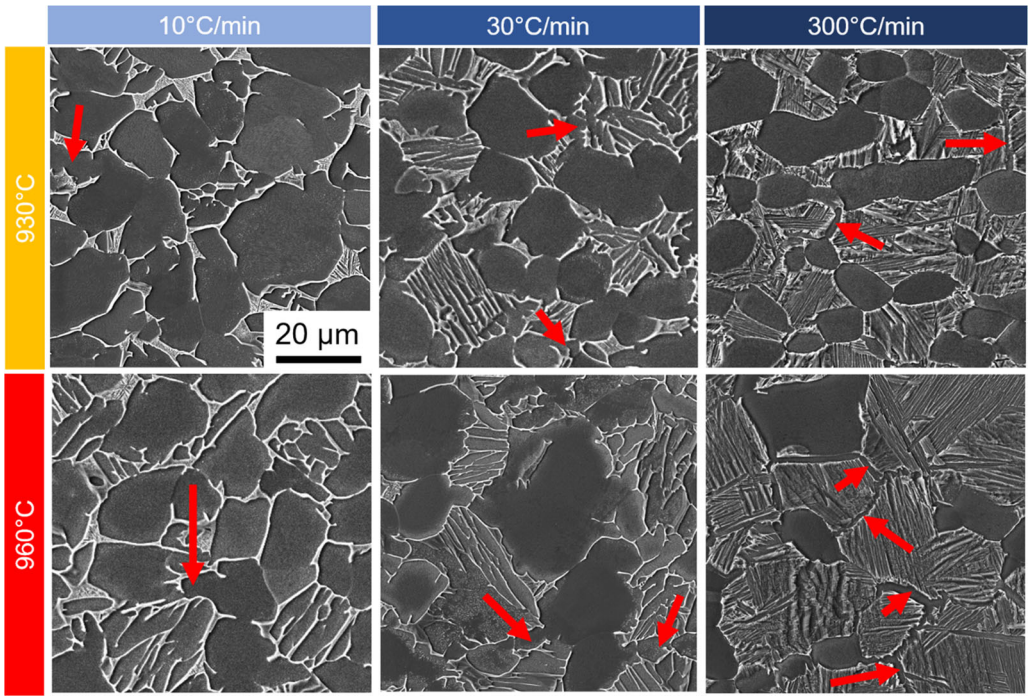

Fig. 4—Representative SE micrographs of the investigated Ti-6Al-4V after holding at 930 °C and 960 °C for 1 h followed by continuous cooling at: 10, 30 and 300 °C/min. The red arrows highlight the α_{GB}.

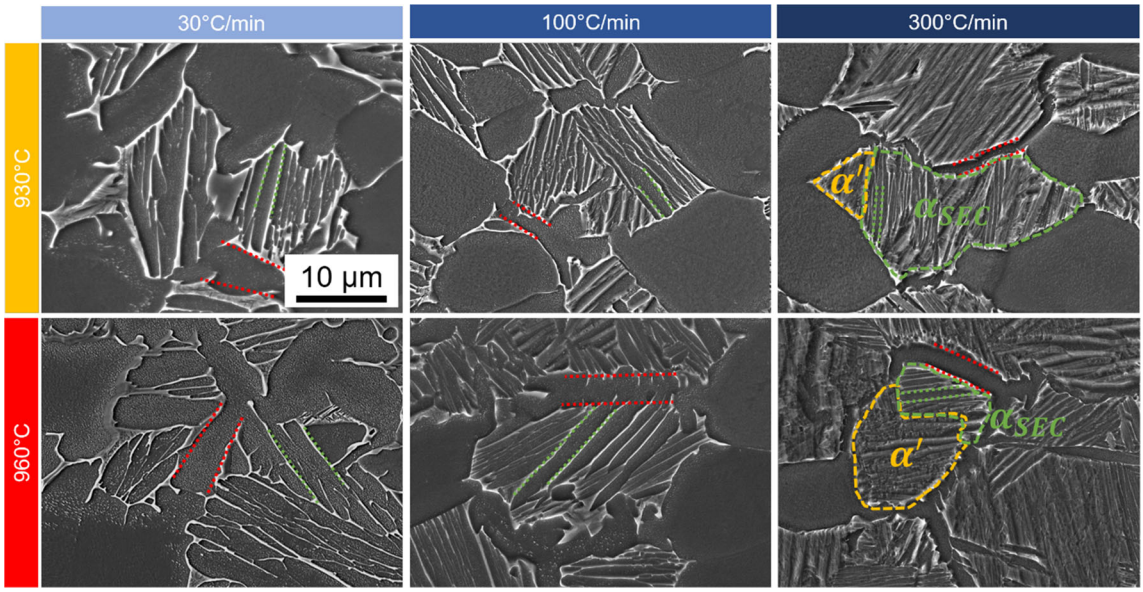

Fig. 5—Representative SE-SEM micrographs of the investigated Ti-6Al-4V after holding at 930 °C and 960 °C for 1 h followed by continuous cooling at 30, 100 and 300 °C/min.

for growth. Since the time for diffusion is higher the slower the cooling rate, the serrations are more pronounced for the 30 °C/minutes compared to 300 °C/minutes. A nearly flat plate-like α_{GB} is observed for the cooling rate of 300 °C/minutes.

Figure 6 illustrates the effect of the cooling rate on the distributions of the diameter of α_P (Figure 6(a)), the circularity of α_P (Figure 6(b)), and the thicknesses of α_{GB} (Figure 6(c)) and α_{SEC} (Figure 6(d)).The distributions were normalized and fitted using a lognormal distribution and only the fitted data are shown in Figure 6. An increase in diameter of α_P with decrease in cooling rate is observed. The circularity of α_P decreases with decreasing cooling rate due to the interface serrations for lower cooling rates. The thickness of α_{GB} or α_{SEC} is smaller with narrower distribution for

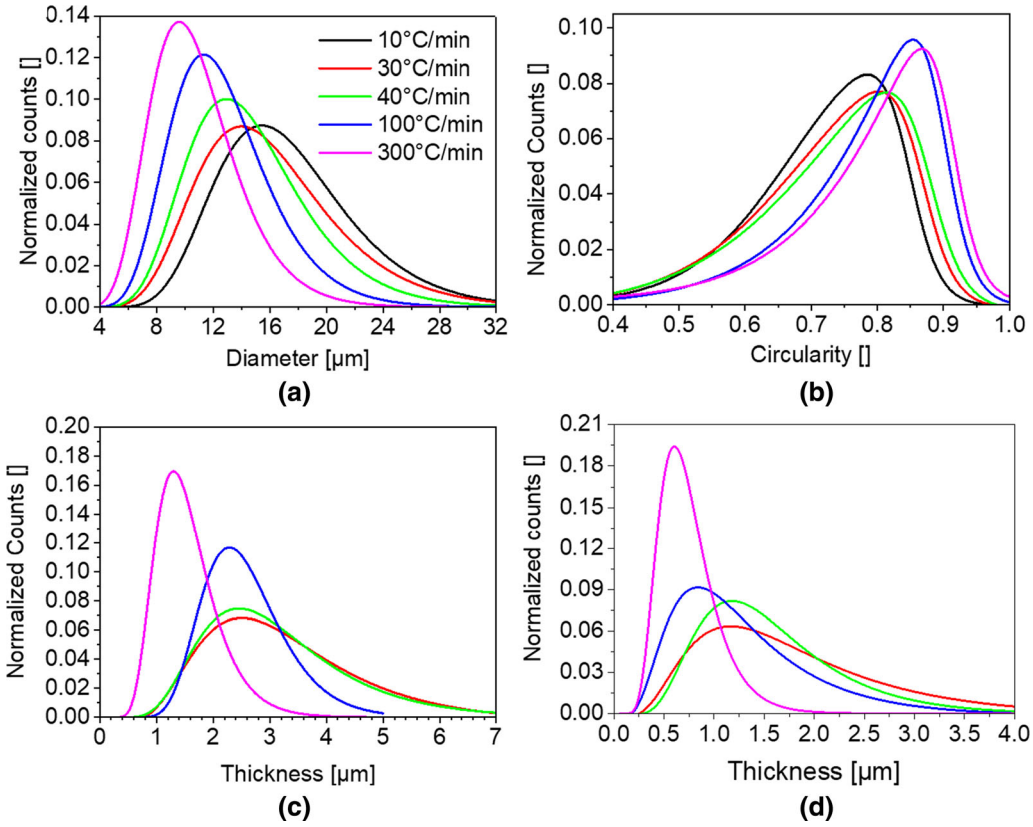

Fig. 6—Normalized distributions of the measured: (*a*) diameter of α_P; (*b*) circularity of α_P; (*c*) thickness of α_{GB}; and (*d*) thickness of α_{SEC}.

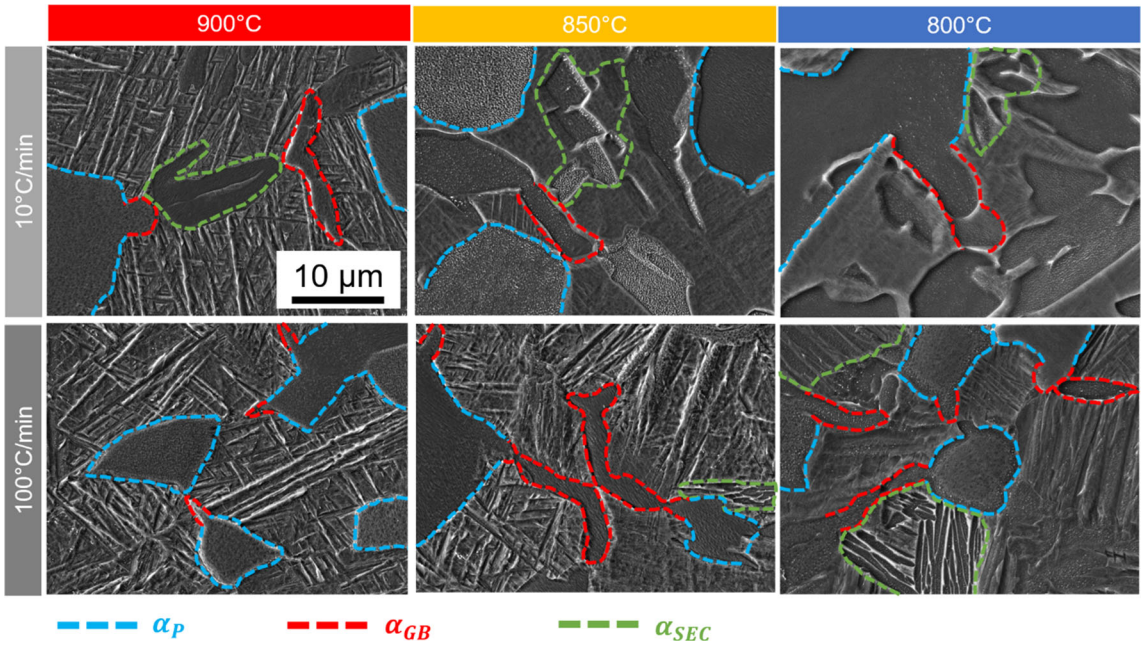

Fig. 7—Representative SE-SEM micrographs of the interrupted heat treatments after holding at 960 °C for 1 h followed by continuous cooling at 10 and 100 °C/min. The tests were interrupted at: 900 °C, 850 °C and 800 °C.

higher cooling rate. The distributions for the cooling rate of 10 °C/minutes are not shown due to the difficulty to distinguish α_P from α_{GB} or α_{SEC}.

2. *Sequence of Phase Formation*

To clarify the sequence of formation of the different morphologies of α-phase, Figure 7 exhibits the typical micrographs after interrupted heat treatments. The α_P,

α_{GB} and α_{SEC} are highlighted in blue dashed line, red dashed line and green dashed line, respectively. The formation of α_{GB} initiates from the globular α_p as well as from triple points of the β grains. The fraction of the grain boundary that is occupied by α_{GB} is very low for 900 °C. At 850 °C the grain boundaries are nearly completely decorated with α_{GB}. Irregular growth of α_{GB} seems to occur at 800 °C and is more pronounced for 10 °C/minutes. Nucleation and growth of α_{GB} do not seem to be significant at temperatures higher than 900 °C for the two investigated cooling rates, leading to comparable evolution behaviour of the α_{GB} after holding at temperatures of 930 °C and 960 °C. Formation of α_{SEC} is not pronounced up to 850 °C. Although Figure 7 shows the presence of α_{SEC} for 10 °C/minutes, its area fraction is notably smaller in comparison to cooling at 100 °C/minutes.

To investigate the growth of the α_{GB} along the β grain boundaries from the α_P, Figure 8 shows the inverse pole figure maps (IPF) of the EBSD measurements for four interrupted heat treatments. The presence of α_{GB} formed from the α_P is highlighted by a dashed white circle. In this case, none or very small (below 2 deg) misorientation angle is observed between the α_P and the formed α_{GB}. The presence of high-angle grain boundaries (boundary misorientation angle higher than 15 deg) is highlighted in white lines. Two nucleation sites were identified for α_{GB} (a) at α_P boundaries as a consequence of a morphological instability due to the presence of an existing $\beta-\beta$ grain boundary, and (b) at β triple points and flat grain boundaries. There is no clear crystallographic relationship between the formed α_{GB} from the α_P and the particle of α_P or at the ones formed at β triple points. It seems that the local supersaturation and surface energy play an important role in the determination of the different nucleation sites. At β triple points, the high surface energy can promote the nucleation of α_{GB}, while the nucleation of α_{GB} at the flat β grain boundaries without α_P is promoted by a high local supersaturation due to large interspacing between the α_P.

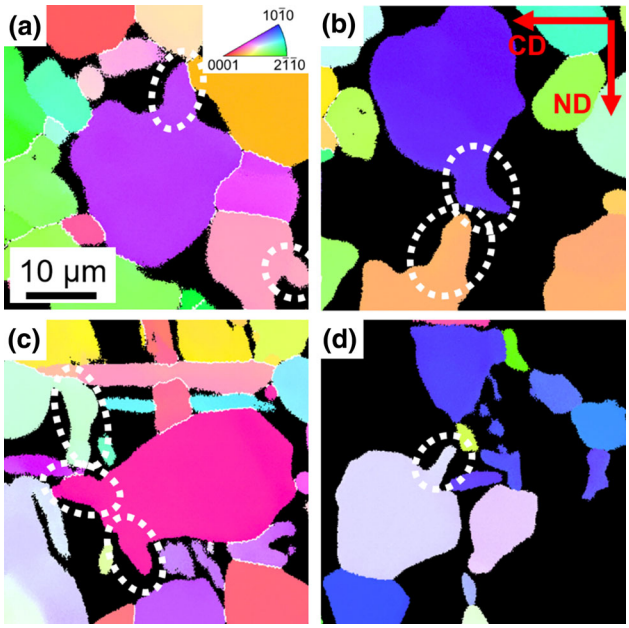

Fig. 8—EBSD-IPF maps with α_P and α_{GB} formed from the α_P indicated by the dashed white circles. The heat treatments correspond to an isothermal for 1 h at 960 °C followed by continuous cooling at (*a*) 10 °C/min interrupted at 800 °C; (*b*) 100 °C/min interrupted at 800 °C; (*c*) 10 °C/min interrupted at 875 °C; (*d*) 100 °C/min interrupted at 875 °C. The martensitic phase was erased for easier visualization. The CD and ND corresponds to cogging and normal direction, respectively.

B. *Model Performance*

The simulated area fraction of α_p, mean α_p diameter, mean thickness of α_{GB} and mean thickness of α_{SEC} are in good agreement with respect to the experimental results. The fitting parameters are in the same range as reported in other investigations.[5,18] The results corroborate with the work of Semiatin *et al.*[4] and Meng *et al.*[5] This work adds the competitive growth of α_P, α_{GB} and α_{SEC}. The nucleation of α_{GB} and α_{SEC} were modelled separately and different free energies for nucleation were considered. Despite of not considering the thermo-history included in the model proposed by Meng *et al.*[5] and despite of not accounting for complex supersaturation fields that are possible to predict when using phase field models,[14] the adoption of a ledge constant to the exact solution showed to be sufficient to achieve notably accuracy in a simple coupled model. The differences between measured and simulated data are dependent on both measurement limitations and model assumptions. The stereological procedures adopted for phase quantification have an inherent error. For instance, the assumption that all α_{SEC} are platelets neglects the amount of α_{SEC} that can exhibit a disc shape or more irregular morphology. Furthermore, the assumption of α_p as isolated spherical particles impacts directly the prediction of the α_p growth. The α_p particles are observed to be partially agglomerated as well as slightly elongated due to initial cogged microstructure. Those differences can explain the deviations and relatively high standard deviation observed in Figure 9.

1. *Influence of the Cooling Rate*

The cooling rate plays an important role in the formation of the different morphologies of α-phase. The following statements can be inferred:

- During continuous cooling, the fraction of α_p increases rapidly until 800 °C (Figures 9(a) and 11(d)). The area fraction of α_p increases for decreasing cooling rate. The model describes accurately the area fraction evolution apart from 30 and 40 °C/minutes for the holding temperature of 960 °C (Figure 9(b)).
- The diameter of α_p increases with decreasing cooling rate (Figures 9(c) and 11(a)).
- The calculated and measured thickness of the α_{GB} are in the range of 1–4 μm and it increases with decreasing cooling rate (Figures 10(a) and (b)). Slightly thicker α_{GB} is observed for the holding temperature of 960 °C. The higher supersaturation

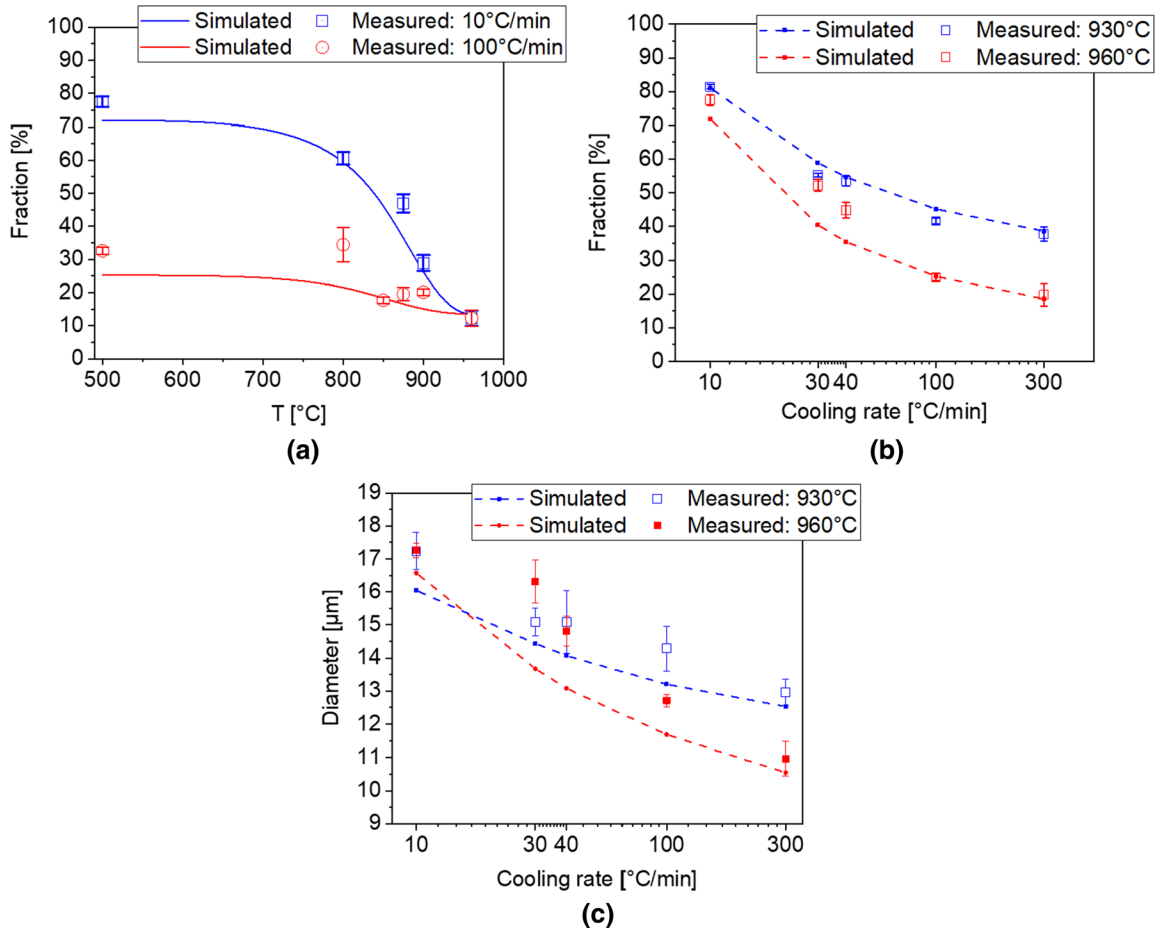

Fig. 9—Measured and modelled evolution of microstructural features during continuous cooling for the α_P: (*a*) average phase fraction at 10 and 100 °C/min for the holding temperatures of 960 °C; (*b*) average phase fraction for the holding temperatures of 930 °C and 960 °C; (*c*) mean diameter for the holding temperatures of 930 °C and 960 °C.

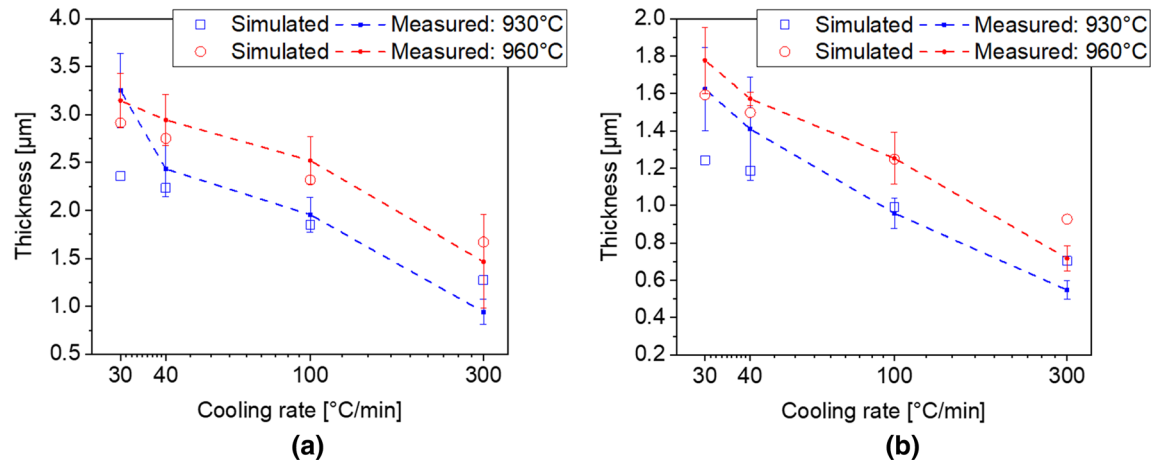

Fig. 10—Measured and modelled evolution of the microstructural features during continuous cooling: (*a*) mean thickness of α_{GB} for the holding temperatures of 930 °C and 960 °C; (*b*) mean thickness of α_{SEC} for the holding temperatures of 930 °C and 960 °C.

grade of the matrix at 960 °C, in addition to the faster growth after nucleation during the initial stages at high temperatures, can explain this difference with respect to the sample cooled from 930 °C.

– The thickness of α_{SEC} was in the range of 0.5 to 2 μm and it increases with decreasing cooling rate (Figures 10(b) and (c)). Since the α_{SEC} is formed at temperatures slightly lower than for the α_{GB}, its

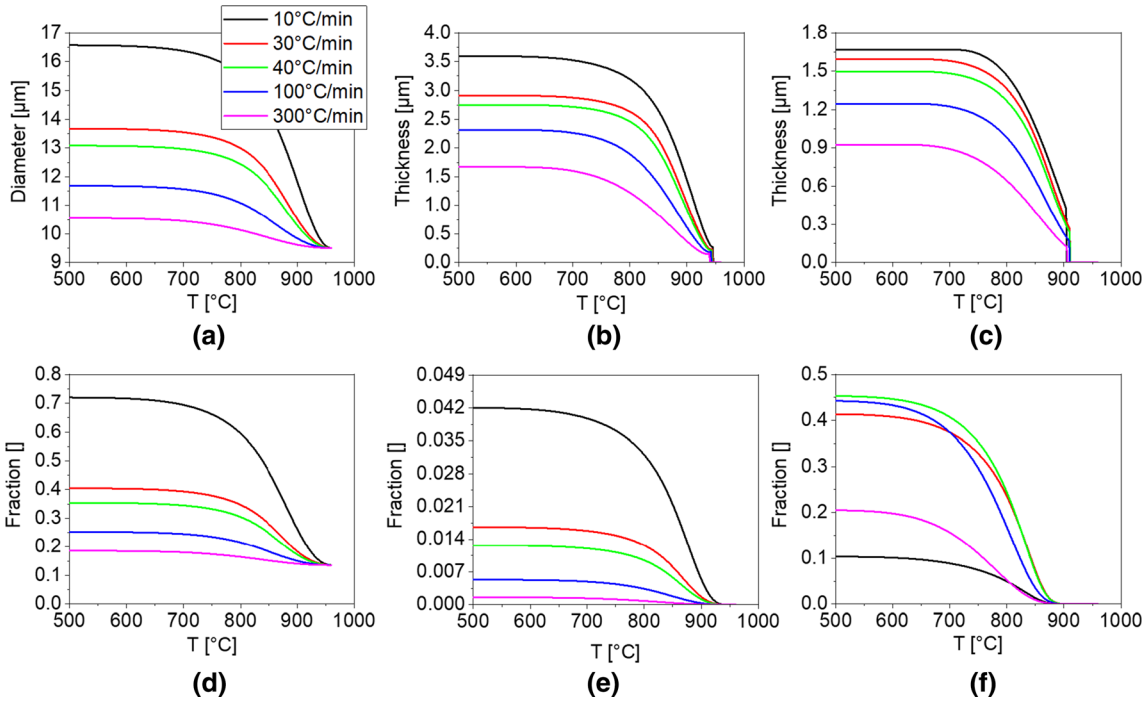

Fig. 11—Simulation results for the holding temperature of 960 °C during continuous cooling: (*a*) mean α_P phase diameter; (*b*) mean thickness of α_{GB}; (*c*) mean thickness of α_{SEC}; (*d*) phase fraction of α_P; (*e*) phase fraction of α_{GB}; (*f*) phase fraction of α_{SEC}.

formation is less influenced by the different holding temperatures.

2. *Evolution of Microstructural Features*

The developed model predicts also the evolution of the microstructural features: mean diameter and area fraction of α_p, mean thickness and area fraction of α_{GB}, and mean thickness and area fraction of α_{GB} and they are plotted in Figure 11 for the holding temperature of 960 °C. The growth of the α-phase morphologies for temperatures lower than 600 °C is negligible. The formation of α_{GB} starts close to 920 °C. Figures 11(b) and (e) show a high growth rate for α_{GB} at around 900 °C, while the growth for temperatures lower than 800 °C is not significant. These evolutions are in good agreement with the experimental observations depicted in Figure 7. The α_{SEC} formation starts at 875 °C, with a significant growth until 700 °C, explaining the micrographs in Figure 7. Figure 11(f) shows that the fraction of α_{SEC} abruptly decreases when the cooling rate increases from 100 to 300 °C/minutes. The low nucleation rate and low time for diffusion explain this behaviour and are confirmed by the presence of martensite in the microstructure after cooling down at 300 °C/minutes. Rae 31 proposed a time-temperature-transformation diagram for Ti-6Al-4V where the martensitic starting temperature is ~850 °C[32] and martensite is formed if this temperature is achieved within ~5 s. To obtain a fully martensitic microstructure, the temperature of ~700 °C should be achieved within ~1 s from the holding temperature.[31] It deviates slightly from the results observed for cooling at 300 °C/minutes, where α_{SEC} is still observed. Although the formation of martensite is not included in the model, the lower formation of α_{SEC} is used as an indication for it.

3. *Additional Physical Features*

Figure 12 shows the nucleation rate of α_{GB} (Figure 12(a)) and α_{SEC} (Figure 12(b)) for the holding temperature of 960 °C. The supersaturation of V within the β-phase matrix is shown in Figure 12(c). The predicted nucleation rate of α_{GB} is significantly smaller compared to α_{SEC} because only the grain boundaries are considered sites for nucleation and formation of α_{GB}. The estimated prior β grain size is 35 μm. Therefore, the density number of platelets of α_{GB} is notably smaller compared to α_{SEC}.

A summary with the temperature for the beginning of nucleation and for the maximum nucleation rate is shown in Table II. The α_{GB} nucleates first compared to α_{SEC}. The temperature for the beginning of nucleation tends to increase with decrease cooling rate. An exception is calculated for the 10 °C/minutes cooling rate. In this case, the predominant growth of α_P leaves no supersaturation to activate earlier nucleation of α_{GB}. Similar tendency is observed for the α_{SEC}. The slightly lower temperatures for nucleation in the case of 10 °C/minutes is more pronounced, as expected due to the higher free energy for nucleation (Eq. [9] in comparison to Eq. [20]). The dependency on the cooling rate in the case of the nucleation rate follows similar behaviour compared to the beginning of nucleation. The temperatures for maximum nucleation rate are 40 °C lower compared to the temperature for the beginning of nucleation for the α_{GB}. In the case of the α_{SEC}, this difference varies between 80 and 100 °C. The

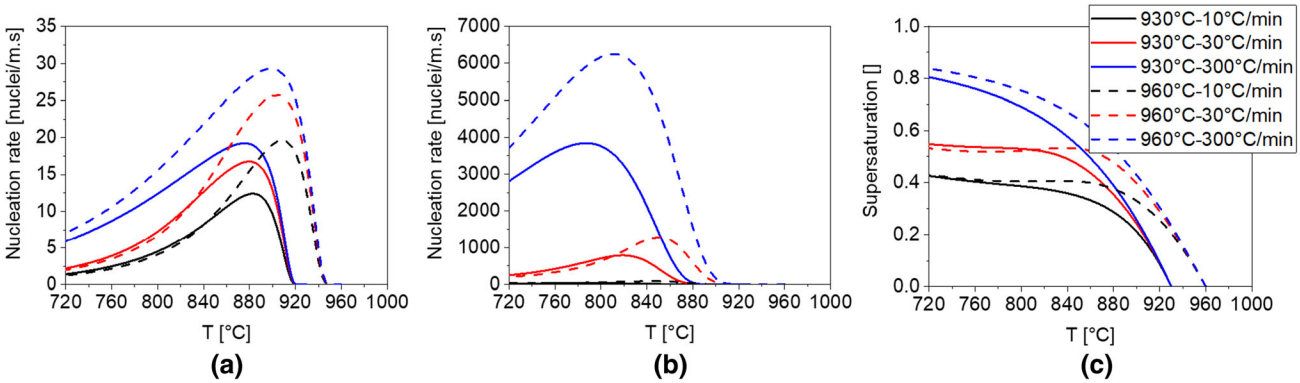

Fig. 12—Simulated results for the holding temperature of 930 °C and 960 °C for the cooling rates of 10, 30 and 300 °C/min: (*a*) nucleation rate of α_{GB}; (*b*) nucleation rate of α_{SEC}; and (*c*) supersaturation of V in the β matrix.

Table II. Approximate Simulated Nucleation Temperatures for the Cooling Rates of 10, 30, 40, 100 and 300 °C/min at Isothermal Treatments at 930 °C and 960 °C

	Temperature for the Beginning of Nucleation [°C]				Temperature for Maximum Nucleation Rate [°C]			
	α_{GB}		α_{SEC}		α_{GB}		α_{SEC}	
Cooling Rate [°C/minutes]	930 °C	960 °C	930 °C	960 °C	930 °C	960 °C	930 °C	960 °C
10	917	945	877	908	883	908	794	846
30	916	944	888	912	880	904	819	851
40	916	944	888	912	879	903	816	847
100	915	942	888	913	877	900	800	829
300	912	940	887	912	876	889	787	811

interrupted heat treatments (Figure 7) showed that α_{SEC} forms at lower temperatures compared to α_{GB}. Similar trend is exhibited by the simulated nucleation rates of α_{SEC}. The incomplete formation of α_{SEC} for high cooling rates (Figures 5 and 11) is also predicted in the current model, since the temperature for maximum nucleation rate of α_{SEC} lies close to 800 °C. Furthermore, the notable low amount of α_{SEC} formed during low cooling rates is also observed (Figure 4) and agrees with the model prediction.

The formation of the different morphologies is driven by the degree of supersaturation of the V in the β-phase, and its evolution during cooling is shown in Figure 12(c). It raises rapidly up to 810 °C, temperature slightly lower compared to the maximum nucleation rate of α_{SEC} (Table II). Moreover, an intensive formation of $\alpha\alpha_{SEC}$ is observed between 850 and 800 °C (Figure 7). Higher supersaturation promotes nucleation of α_{GB} and α_{SEC} as well as growth of α_P. The simulation and the microstructure analysis show that the growth of α_P is favourable for lower cooling rates, while formation of α_{SEC} is promoted for higher cooling rates. The lower time for diffusion at high cooling rates increases the supersaturation of V of the β matrix, thus promoting the formation of α_{SEC}. The long time for diffusion for low cooling rates promotes the growth of α_P.

IV. SUMMARY AND CONCLUSIONS

The sequence of formation and growth of the different morphologies of α-phase (primary, secondary and allotriomorphic) in Ti-6Al-4V were investigated during cooling from isothermal treatments below the β-transus temperature. A mesoscale physical model to account for the competitive growth of the different morphologies was developed. Nucleation and growth of α_{GB} as well as of α_{SEC} are modelled based on the nucleation and growth of platelets. The growth of α_P is modelled as the growth of a spherical particle. The simulated results are in agreement with the obtained results and the following conclusions are inferred:

- Growth of α_P is more pronounced for low cooling rates and occurs more notable up to 800 °C
- Regular (planar) interface shape of α_{GB} is observed decorating the prior β grain boundaries for high cooling rates. For low cooling rates, irregular shapes are observed
- α_{GB} nucleates preferentially from existing α_p phase. For higher cooling rates nuclei in triple points of the β grains and other regions of the prior β/β grain boundary are observed. The higher nucleation rate for those cooling rates can explain the different behaviour

- Formation of α_{SEC} occurs at a lower temperature for the same cooling rate compared to the formation of α_{GB}. The predicted temperature for maximum nucleation rate of α_{GB} is ~80 °C higher compared to the one for the maximum nucleation rate of α_{SEC}
- α_{SEC} nucleates from the already existing α_{GB} as well as at the interface with the α_P
- The variation of nucleation rate with respect to the cooling rate is notably more pronounced for the α_{SEC} compared to α_{GB}
- A sharp increase of V supersaturation in the β matrix is observed up to 850 °C, which is attributed to contributing to the formation of α_{SEC}, especially for cooling rates higher than 10 °C/minutes.

ACKNOWLEDGMENTS

Open access funding provided by Graz University of Technology. The authors carried out this work under CD-Laboratory for Design of High-Performance Alloys by Thermomechanical Processing, supported by the Christian Doppler Society.

OPEN ACCESS

APPENDIX

A Matlab® routine was developed to implement the model to couple the growth of the α_p and the formation and growth of α_{GB} and α_{SEC}. The used parameters are listed in Table A1.

Table A1. List of the Parameters Used for the Modelling of the Growth of α_P and Formation and Growth of α_{GB} and α_{SEC}

Description	Parameter	Value	Reference
V Concentration in the Alloy	C_0	4.21	chemical composition measurement
V Concentration in α-Phase	C_P, $C_P^{\alpha_{GB}}$, $C_P^{\alpha_{SEC}}$	2.0	[6]
V Concentration at the α/β Interface	C_I	function of temperature	calculated with JMatPro® v.10
Pre-exponent Nucleation Parameter for α_{GB}	N_{0GB}	function of prior β grain size: $6.9 \times 10^4 \left(\frac{GS_0}{GS}\right)^{0.5}$	empirical from this work
Reference Grain Size for the Nucleation of α_{GB}	GS_0	35 μm	fitting parameter. this work
Pre-exponent Nucleation Parameter for α_{SEC}	N_{0SEC}	$6x10^7$	fitting parameter. this work
Parameter for Activation Energy of Nucleation for α_{GB}	A^*_{GB}	$2.79x10^3$	fitting parameter. this work
Parameter for Activation Energy of Nucleation for α_{SEC}	A^*_{SEC}	$8.35x10^3$	fitting parameter. this work
Parameter for Activation Energy of Nucleation for Sympathetic Growth	A_{SYM}	$1.39x10^4$	[5]
Parameter for Activation Energy for Nucleation at α/β Interface	$A_{\alpha\beta}$	$1.27x10^3$	[20]
α/β Interface Energy	$\gamma_{\alpha\beta}$	0.10 J/m^2	[20]

Table A1. continued

Description	Parameter	Value	Reference
α/α Interface Energy	$\gamma_{\alpha\alpha}$	0.30 J/m^2	[5]
Ti atomic Volume	V_m	$1.0896x10^{-5}$	[5]
Shape Factor	$S(\theta)$	0.001728	[20]
Activation Energy for Diffusion	Q	145.17 kJ/mol	[6]
Activity Coefficient	$\frac{\partial V}{\partial C_I}\frac{C_I}{V}$	0.9	[6]
Ledge Coefficient for α_{GB} Growth	m_{GB}	5	ftting parameter. this work
Ledge Coefficient for α_{SEC} Growth	m_{SEC}	3	fitting parameter. this work

REFERENCES

1. G. Lütjering and J.C. Williams: *Titanium*, Heidelberg, Springer, Berlin Heidelberg, Berlin, 2007.
2. R. Pederson: Microstructure and Phase Transformation of Ti-6Al-4V, PhD Dissertation, Lulea University of Technology, Lulea, Sweden, 2002.
3. X. Gao, W. Zeng, S. Zhang, and Q. Wang: *Acta Mater.*, 2017, vol. 122, pp. 298–309.
4. S. L. Semiatin, S. L. Knisley, P. N. Fagin, F. Zhang, and D. R. Barker: *Metall. Mater. Trans. A,* 2003, vol. 34 A(10), pp. 2377–86.
5. M. Meng, X.G. Fan, H. Yang, L.G. Guo, M. Zhan, and P.F. Gao: *J. Alloys Compd.*, 2017, vol. 714, pp. 294–302.
6. Z. Sun, X. Li, H. Wu, and H. Yang: *J. Alloys Compd.*, 2016, vol. 689, pp. 693–701.
7. N. Kherrouba, M. Bouabdallah, R. Badji, D. Carron, and M. Amir: *Mater. Chem. Phys.*, 2016, vol. 181, pp. 462–69.
8. M. Enomoto, H.I. Aaronson, and T. Furuhara: *MetallTrans. A*, 1991, vol. 22 (6), pp. 1341–48.
9. E.S.K. Menon and H.I. Aaronson: *MetallMater. Trans. A*, 1986, vol. 17 (10), pp. 1703–15.
10. C. Atkinson: *MetallTrans. A*, 1991, vol. 22 (6), pp. 1211–18.
11. M. Enomoto: *MetallTrans. A*, 1991, vol. 22 (6), pp. 1235–45.
12. K. J. Song, Y. H. Wei, Z. B. Dong, X. Y. Wang, W. J. Zheng, and K. Fang: *J. Phase Equilibria Diffus.*, 2015, vol. 36(2), pp. 136–48.
13. Q. Chen, N. Ma, K. Wu, and Y. Wang: *Scr. Mater.*, 2004, vol. 50 (4), pp. 471–76.
14. B. Appolaire, L. Héricher, and E. Aeby-Gautier: *Acta Mater.*, 2005, vol. 53 (10), pp. 3001–11.
15. G. W. Mei Yang Tao Liu, Wen-Juan Zhao, Dong-Sheng Xu: *Acta Metallurgica Sinica(English letters)*, 2017, vol. 30(8), pp. 745–52.
16. M. Meng, H. Yang, X.G. Fan, S.L. Yan, A.M. Zhao, and S. Zhu: *J. Alloys Compd.*, 2017, vol. 691, pp. 67–80.
17. V. Raghavan: *Solid State Phase Transformations*, PHI Learning Private Limited, Delhi, 1987.
18. I. Katzarov, S. Malinov, and W. Sha: *MetallMater. Trans. A*, 2002, vol. 33 (4), pp. 1027–40.
19. P. Homporová: Thermal history of alpha morphology in titanium alloy Ti-6Al-4V, PhD Dissertation, Vienna University of Technology, Vienna, 2011.
20. J. Tiley, E. Lee, S. Kar, R. Banerjee, J.C. Russ, and H.L. Fraser: *Mater. Sci. Eng., A*, 2004, vol. 372(1-2), pp. 191–98.
21. GIMP - GNU Image Manipulation Program, https://www.gimp.org/. Accessed: 20-Aug-2019.
22. ImageJ, https://imagej.nih.gov/ij/. Accessed: 20-Aug-2019.
23. U. Zwicker: *Titan und Titanlegierungen*, Springer, Berlin Heidelberg, 1974.
24. M. Villa, J.W. Brooks, R.P. Turner, H. Wang, F. Boitout, and R.M. Ward: *Metall. And Mater. Trans. B*, 2019, vol. 50, pp. 2898–11.
25. R. Shi, Y. Wang: *Acta Mater.*, vol. 61(16), pp. 6006–24.
26. M. Enomoto and H.I. Aaronson: *MetallTrans. A*, 1986, vol. 17 (8), pp. 1385–97.
27. E. Sarath Kumar Menon, H.I. Aaronson: *Metall. Mater. Trans. A*, 1986, vol. 17(10), pp. 1703–15.
28. D.S. Wilkinson: *Mass Transport in Solids and Fluids*, Cambridge University Press, Cambridge, 2000.
29. J.W. Christian: *The Theory of Transformations in mEtals and Alloys: An Advanced Textbook in Physical Metallurgy*, Pergamon Press, Oxford, 1975.
30. A. Deschamps and Y. Brechet: *Acta Mater.*, 1998, vol. 47 (1), pp. 293–305.
31. W. Rae: *Mater. Sci. Technol.*, 2019, vol. 35 (7), pp. 747–66.
32. J. Sieniawski, W. Ziaja, K. Kubiak, M. Motyka: *in Titanium alloys-advances in properties control. IntechOpen*, 2013.